CrossMark

Water-rich Disks around Late M Stars Unveiled: Exploring the Remarkable Case of Sz 114

Chengyan Xie[1], Ilaria Pascucci[1], Feng Long[1,17], Klaus M. Pontoppidan[2], Andrea Banzatti[3], Anusha Kalyaan[3], Colette Salyk[4], Yao Liu[5], Joan R. Najita[6], Paola Pinilla[7], Nicole Arulanantham[8], Gregory J. Herczeg[9], John Carr[10], Edwin A. Bergin[11], Nicholas P. Ballering[12], Sebastiaan Krijt[13], Geoffrey A. Blake[14], Ke Zhang[15], Karin I. Öberg[16], and Joel D. Green[8]
the JDISCS collaboration

[1] Lunar and Planetary Laboratory, The University of Arizona, Tucson, AZ 85721, USA; cyxie@arizona.edu
[2] Jet Propulsion Laboratory, California Institute of Technology, 4800 Oak Grove Drive, Pasadena, CA 91109, USA
[3] Department of Physics, Texas State University, 749 North Comanche Street, San Marcos, TX 78666, USA
[4] Department of Physics and Astronomy, Vassar College, 124 Raymond Avenue, Poughkeepsie, NY 12604, USA
[5] Purple Mountain Observatory & Key Laboratory for Radio Astronomy, Chinese Academy of Sciences, 10 Yuanhua Road, Nanjing 210023, People's Republic of China
[6] NSF's NOIRLab, 950 North Cherry Avenue, Tucson, AZ 85719, USA
[7] Mullard Space Science Laboratory, University College London, Holmbury St Mary, Dorking, Surrey RH5 6NT, UK
[8] Space Telescope Science Institute, 3700 San Martin Drive, Baltimore, MD 21218, USA
[9] Kavli Institute for Astronomy and Astrophysics, Peking University, Yi He Yuan Lu 5, Haidian Qu, 100871 Beijing, People's Republic of China
[10] Department of Astronomy, University of Maryland, College Park, MD 20742, USA
[11] Department of Astronomy, University of Michigan, Ann Arbor, MI 48109, USA
[12] Department of Astronomy, University of Virginia, Charlottesville, VA 22904, USA
[13] School of Physics and Astronomy, University of Exeter, Stocker Road, Exeter EX4 4QL, UK
[14] Division of Geological and Planetary Sciences, California Institute of Technology, MC 150-21, 1200 East California Boulevard, Pasadena, CA 91125, USA
[15] Department of Astronomy, University of Wisconsin–Madison, 475 North Charter Street, Madison, WI 53706, USA
[16] Center for Astrophysics, Harvard & Smithsonian, 60 Garden Street, Cambridge, MA 02138, USA

Abstract

We present an analysis of the JDISCS JWST/MIRI-MRS spectrum of Sz 114, an accreting M5 star surrounded by a large dust disk with a shallow gap at $\sim$39 au. The spectrum is molecule-rich; we report the detection of water, CO, CO_2, HCN, C_2H_2, and H_2. The only identified atomic/ionic transition is from [Ne II] at 12.81 μm. A distinct feature of this spectrum is the forest of water lines with the 17.22 μm emission surpassing that of most mid-to-late M star disks by an order of magnitude in flux and aligning instead with disks of earlier-type stars. Moreover, the flux ratios of C_2H_2/H_2O and HCN/H_2O in Sz 114 also resemble those of earlier-type disks, with a slightly elevated CO_2/H_2O ratio. While accretional heating can boost all infrared lines, the unusual properties of Sz 114 could be explained by the young age of the source, its formation under unusual initial conditions (a large massive disk), and the presence of dust substructures. The latter delays the inward drift of icy pebbles and helps preserve a lower C/O ratio over an extended period. In contrast, mid-to-late M-star disks—which are typically faint, small in size, and likely lack significant substructures—may have more quickly depleted the outer icy reservoir and already evolved out of a water-rich inner disk phase. Our findings underscore the unexpected diversity within mid-infrared spectra of mid-to-late M-star disks, highlighting the need to expand the observational sample for a comprehensive understanding of their variations and thoroughly test pebble drift and planet formation models.

1. Introduction

Observations of disks around young stars provide a unique opportunity to witness planet formation in action (e.g., Bae et al. 2023) and constrain the distribution of volatiles while planets are assembling (e.g., Öberg & Bergin 2021). Spitzer/ IRS observations at moderate resolution ($R \sim 700$) mostly targeted young solar analogs (FGK and early M) and

demonstrated that their disk atmospheres are rich in volatiles. Most of the volatile oxygen and carbon are carried by H_2O and CO, while most nitrogen is likely in the undetected form of gas-phase N_2 (e.g., Pontoppidan et al. 2014, and references therein). For the brightest disks, high-resolution ($R \sim 25,000–95,000$) ground-based telescopes targeted few accessible transitions and spectroscopically confirmed that infrared molecular emission mostly traces gas within a few au from the star (e.g., Pontoppidan et al. 2010; Mandell et al. 2012; Najita et al. 2018; Salyk et al. 2019; Banzatti et al. 2023b). This is the gas inside the water-ice line (hereafter the snowline) that is accreted by those gaseous planets, including sub-Neptunes, within $\sim$1 au (e.g., Bean et al. 2021; Izidoro et al. 2022).

---

[17] NASA Hubble Fellowship Program Sagan Fellow.

In contrast to young solar analogs, only a handful of mid-to-late M-star disks (disks around stars whose spectral types are later than $\sim$M3) have IRS spectra and only at modest signal-to-noise ratios (S/Ns) due to their relatively low luminosity. Nevertheless, their infrared spectra are different and characterized by (i) stronger C_2H_2 than HCN emission, a signature seen even in lower-resolution IRS spectra (Pascucci et al. 2009), and (ii) weak/undetected H_2O lines (Pascucci et al. 2013). Retrieval slab models of gas in local thermodynamic equilibrium (LTE) suggest that the inner disk has an enhanced abundance of C_2H_2 and HCN relative to water (Pascucci et al. 2013), pointing to elevated C/O ratios of $\sim$1 (e.g., Najita et al. 2011). In contrast, when the same models are applied to disks around earlier-type stars, C_2H_2 and HCN are typically orders of magnitude less abundant than H_2O (e.g., Carr & Najita 2011; Salyk et al. 2011; Walsh et al. 2015). A similar chemical trend has also been reported with the Atacama Large Millimeter/submillimeter Array (ALMA) for the outer disks ($\geqslant$20 au) of five late M stars whose C_2H/HCN column density ratios are a factor of a few higher than in disks around earlier-type stars[18] (Pegues et al. 2021).

These findings hint at a change in the volatile content of mid-to-late M-star disks, with hydrocarbons and nitriles likely being more abundant than in disks around earlier-type stars. Supporting this inference, the first JWST Mid-Infrared Instrument (MIRI) Medium Resolution Spectrometer (MRS) spectrum ($R \sim 2000$) of an early M-star (M1.5, $M_* \sim 0.5\,M_\odot$; Andrews et al. 2018) disk shows solar-like H_2O, C_2H_2, and HCN abundances (GW Lup; Grant et al. 2023), while that of a late M-star (M5; $M_* \sim 0.2\,M_\odot$) disk has no water detection but strong emission from C-bearing molecules, including benzene, C_6H_6 (2MASS J16053215–1933159, hereafter J160532; Tabone et al. 2023). However, the selection of these two disks was based on the availability of Spitzer/IRS spectra at $R \sim 700$, which provided the foundation for the aforementioned identified trends. As it is difficult to draw any firm conclusion from such a small sample, targeting disks that have not been previously observed with Spitzer/IRS is essential, particularly for the underrepresented late M stars, as it allows for a comprehensive exploration of the potential diversity within this class.

Here, we present the JWST/MIRI-MRS spectrum of the disk of Sz 114, an accreting M5 star ($M_* \sim 0.17\,M_\odot$; e.g., Hughes et al. 1994; Mortier et al. 2011; Alcalá et al. 2017) located in the Lupus III subgroup (median distance of 158.9 pc and median age of 2.5 Myr; Galli et al. 2020). This disk, which is massive ($M_{dust} \sim 30\,M_\oplus$; Ansdell et al. 2018) and millimeter-bright, was observed as part of the ALMA Disk Substructures at High Angular Resolution Project (DSHARP; Andrews et al. 2018) and found to have a shallow dust gap at $\sim$39 au (Huang et al. 2018). Follow-up visibility modeling using the super-resolution code `frank` suggests additional unresolved substructures between $\approx$7 and 12 au (Jennings et al. 2022). Sz 114 was not observed with Spitzer/IRS at $R \sim 700$. We show here that the mid-IR spectrum of this late M-star disk is remarkably water-rich (Sections 2 and 3). We discuss molecular flux ratios relative to water in the context of other mid-to-late M-star disks, as well as disks around earlier-type stars observed with Spitzer/IRS and JWST/MIRI-MRS. We propose that the rich water spectrum of Sz 114 is driven by the star's relatively high

accretion luminosity in combination with a young age and a more massive large disk with substructures that might prolong the inward drift of icy pebbles (Section 4). We conclude in Section 5 by summarizing the key findings of our study. Additionally, we emphasize the importance of expanding the sample of mid-to-late M-star disks beyond that observed with Spitzer/IRS. The extension to systems with a range of ages, accretion luminosities, and outer disk substructures is crucial for capturing the diversity of inner M-star disks and thoroughly testing our current understanding of pebble drift and planet formation.

2. Observations and Data Reduction

Sz 114 was observed with the MRS (Wells et al. 2015) of the JWST-MIRI (Rieke et al. 2015) as part of the Cycle 1 Treasury Project "A DSHARP-MIRI Treasury Survey of Chemistry in Planet-forming Regions" (ID: 1584, PI: C. Salyk, co-PI: K. Pontoppidan) in the JWST Disk Infrared Spectral Chemistry Survey (hereafter JDISCS). To minimize fringes, the source was first acquired using the MRS target acquisition procedure with a neutral density filter. This procedure identifies the brightest pixel in the image and offsets it to the integral field unit's center with an accuracy of 0″.1. JDISCS employed the four-point dither pattern, which is optimized for point sources, in the negative direction; i.e., the pattern moves from the bottom right to top left. All three MIRI-MRS grating settings were selected to ensure full spectral coverage (4.9–28 μm). To achieve an S/N of $\sim$100 at the longest wavelengths, 75 groups per ramp were selected for an exposure time per module of 832.5 s.

The data were reduced following Pontoppidan et al. (2023). In short, the JWST Calibration Pipeline (Bushouse et al. 2022) version 1.11.0 and Calibration Reference Data System context jwst_1105.pmap were used to process the data up to stage 2, resulting in data cubes for every exposure, channel, and subband. The 1D spectra were extracted with an aperture that widens linearly with wavelength within each subband, and the background was subtracted from the two opposing dither positions. Then the spectra were individually divided by a relative spectral response function constructed from the asteroid 515 Athalia (PID: 1549; PI: K. Pontoppidan) before median clipping of the four dither positions. Finally, we shifted the spectrum by $-1\,\mathrm{km\,s^{-1}}$ to align the lines with the mean heliocentric radial velocity of the Lupus III subgroup, where Sz 114 is located (Galli et al. 2013). The final reduced spectrum is shown in black in Figure 1.

3. The Water-rich Mid-infrared Spectrum of Sz 114

The MIRI-MRS spectrum of Sz 114 shows a broad and flat-topped 10 μm silicate emission feature typical of mid-to-late M-star disks (e.g., Apai et al. 2005; Pascucci et al. 2009). These properties indicate that the typical dust grains in the disk atmosphere are microns in size, i.e., about 10 times larger than interstellar medium dust and typical grains in solar-type disk atmospheres (e.g., Natta et al. 2007). In addition, the prominent rovibrational bands from C_2H_2, HCN, and CO_2, all of which were previously detected with Spitzer/IRS in mid-to-late M-star disks (Pascucci et al. 2009, 2013), are also present in the Sz 114 MIRI-MRS spectrum; see Figure 1. At the shortest wavelengths, several CO $\nu = 1 - 0$ P-branch lines are also found, while CO emission in disks has often been found to

---

[18] Unlike C_2H_2, C_2H has a permanent dipole moment and hence millimeter transitions.
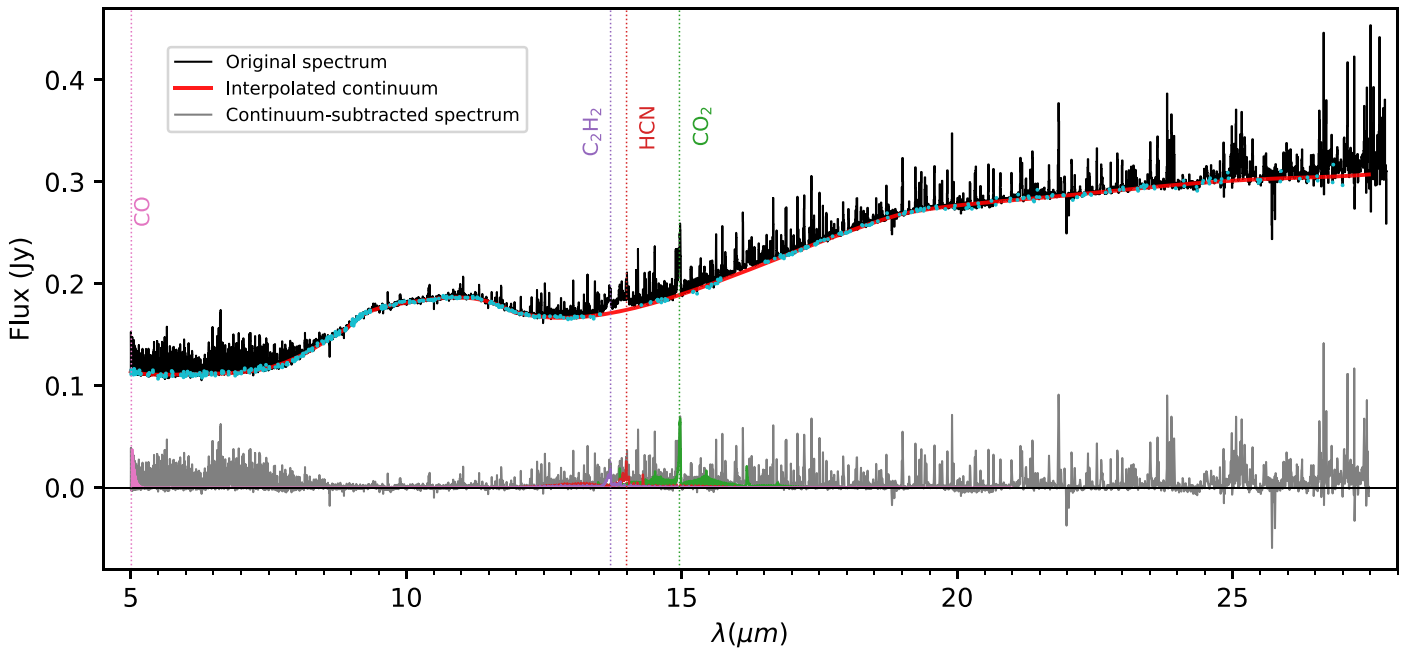
Figure 1. Reduced MIRI-MRS spectrum of Sz 114 (black). The continuum (red line) is interpolated at the light blue dots and superimposed on the original spectrum. The continuum-subtracted spectrum is shown below in gray. The spectrum is dominated by water emission lines, and wavelengths of other prominent molecular rovibrational bands are indicated as vertical lines. The dips at ∼19, ∼22, and ∼26 μm are not real but rather data reduction artifacts.

have non–local thermodynamic equilibrium excitation (e.g., Thi et al. 2013; van der Plas et al. 2015).
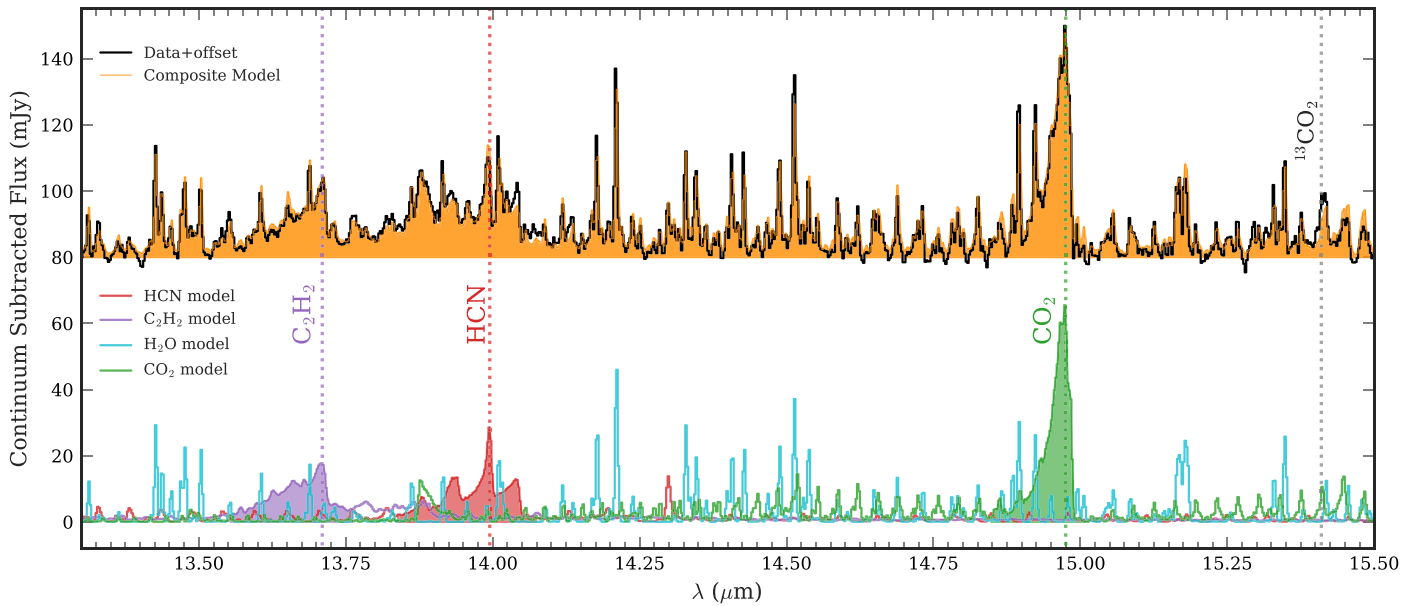
The most prominent characteristic of this spectrum is the forest of water lines, from the hot bending rovibrational band at ∼6.6 μm to the cooler pure rotational lines at longer wavelengths (see, e.g., Figure 1 in Banzatti et al. 2023b). In relation to water emission, Sz 114 is very different from other mid-to-late M-star disks observed with Spitzer/IRS (Pascucci et al. 2013) and the similarly late M5 object recently observed with MIRI-MRS (J160532; Tabone et al. 2023) in which water emission was either very weak or absent. Such a rich water spectrum is more akin to that of disks around earlier-type stars (spectral types earlier than M3; e.g., Carr & Najita 2011; Salyk et al. 2011), as discussed further in Section 4. Visual inspection of the MIRI data cubes does not show any extended emission. Therefore, as in previous papers (e.g., Salyk et al. 2011; Pascucci et al. 2013), we assume that the water emission is tracing the disk surface instead of jets or winds.

Properly identifying weak emission lines from other molecules requires subtracting the dust continuum emission and the rich water spectrum. To identify line-free channels for continuum subtraction, we first generated a water spectrum with CLIcK (Liu et al. 2019). CLIcK assumes a plane-parallel slab of gas in LTE and adopts molecular parameters from the HITRAN database (e.g., Gordon et al. 2022). Line overlap is properly accounted for using Equation (1) in Tabone et al. (2023). With the generated water spectrum, we identified by eye continuum regions that avoided water lines and the prominent rovibrational bands mentioned above (see light blue points in Figure 1). After experimenting with fits with polynomials of different orders, we found that a fifth-order polynomial provides a good fit for the entire continuum emission.[19] The continuum-subtracted spectrum of Sz 114 is depicted in gray below the original spectrum in Figure 1.

Next, we work with the continuum-subtracted spectrum and run CLIcK again to find the water models that best fit the water emission between ∼10 and 19 μm. The reason for focusing on this restricted wavelength range is that it contains the rovibrational bands of interest for placing Sz 114 in the context of other disks observed with Spitzer/IRS and, more recently, JWST/MIRI-MRS (see Section 4). In spite of the restricted wavelength range, the water spectrum covers a broad range of upper energy levels and Einstein-A coefficients that may not be fitted well by a single-temperature slab of gas in LTE (e.g., Banzatti et al. 2023a). This is indeed the case for Sz 114, where we find that two temperatures are necessary to reproduce the observed spectrum (see the sum of the two slab models as light blue lines in the bottom panel of Figure 2 and in Figure 3). The best fit is found by first fitting the hot water in the region between ∼10 and 12 μm and the high-energy line at 15.18 μm ($E_{\rm up} \sim$ 8000 K) simultaneously. Next, the best fit to the hot water is removed, and then all water lines are fitted between ∼10–12 and ∼16.3–19 μm, excluding regions with known molecular lines other than water. We stress that the aim of this modeling is not to perfectly match the complete JWST-MIRI spectrum. Instead, our goal is merely to identify a suitably precise model within the molecular feature-rich range (∼13–17 μm) to untangle the contribution from individual molecules and measure their line fluxes.

These slab models have three input parameters: the emitting radius ($R_{\rm em}$; the model fits for an equivalent area of $\pi R_{\rm em}^2$), the column density (N), and the gas temperature (T). To fit the water lines, we generate a grid of 4000 models using a custom-written random walk python code (see Appendix A for more details) with starting values $R_{\rm em} = 0.2$ au, $N = 10^{18}$ cm^{-2}, and $T = 1000$ K for the hot and 300 K for the cool components, based on prior models of solar-type disks (Banzatti et al. 2023b). For each step, random values are chosen between ±0.05 au for $\Delta R_{\rm em,i}$, ±2 for $\ln(\Delta N_i)$, and ±100 K for ΔT_i. Using Equation (2) in Mulders et al. (2015) with M_* and $\dot{M}_{\rm acc}$

---

[19] We used `curvefit` within `scipy` (Virtanen et al. 2020b) for the optimization.

Figure 2. Upper panel: composite model (orange shaded region) between 13.4 and 15.5 μm compared to the Sz 114 JWST-MIRI spectrum (black). Lower panel: individual best fits to water, C_2H_2, HCN, and CO_2.

for Sz 114 (Table 1) and assuming typical values for the Rosseland mean opacity (from 20 to 570 cm^2 g^{-1}), a gas-to-dust ratio of 100, and two values for the turbulent mixing strength (0.01 and 0.001), we estimate the midplane snowline to be between $\sim$0.1 and 0.5 au. Since the cool component is still at several hundred K, we set an upper limit of 0.5 au for R_{em}; i.e., most of the water emission is coming within the snowline. The best-fit model is the one with the minimum χ^2, and the derived temperatures, column densities, and emitting radii are summarized in Table 3 of Appendix A.

After subtracting the water spectrum, we proceed to fit the next major molecular emitters in the 10–19 μm region with CLIcK. First, we fit the CO_2 spectrum between 14.6 and 15.4 μm, thus covering many P- and R-branches in addition to the strongest Q-branch emission; see Figure 3. Next, we remove the best-fit spectrum extended to the entire wavelength region and fit together the C_2H_2 and HCN rovibrational bands between 13.5 and 14.3 μm. The best-fit parameters for these molecular species are also summarized in Table 3 of Appendix A, while the composite model compared to the data is shown in the upper panel of Figure 2, with individual molecular emission models in the lower panel.

Aware of the degeneracies among parameters even at the sensitivity and spectral resolution of MIRI-MRS (e.g., Grant et al. 2023), we use these fits merely to separate the contribution from different molecules and calculate line fluxes. The fluxes are calculated by integrating the data (or model for the blended molecules C_2H_2, HCN, and CO_2) within the wavelength range reported in Table 2. To facilitate the comparison between Sz 114 and literature sources, these ranges are chosen to match those adopted in Spitzer studies (e.g., Salyk et al. 2011). Regarding water, we note that the two tentative detections in late M-star disks are at 17.22 μm (in 2MASS J04381486+2611399 and 2MASS J04442713 +2512164, hereafter J043814 and J044427; see Pascucci et al. 2013); hence, we focus on the flux of this line for Sz 114. The calculated line fluxes can be found in Table 2. Because the disk surface snowline is further out than the midplane

snowline, we have also run models that do not restrict R_{em} to be within $\sim$0.5 au. Although the best-fit values for T and N are different from those reported in Table 3, the molecular line fluxes, which are the focus of this paper, are within 5% of those reported in Table 2.

Inspection of the continuum-subtracted spectrum with the best-fit water, CO_2, C_2H_2, and HCN synthetic models reveals additional molecular transitions (see Table 2): two from H_2 and a tentative detection of the rovibrational band from the rarer isotopologue $^{13}CO_2$ at $\sim$15.41 μm (see Grant et al. 2023 for a stronger detection in GW Lup). We have also searched for C_4H_2, C_6H_6, and CH_4, since they were detected toward J160532 with MIRI-MRS (Tabone et al. 2023), but did not identify them in the spectrum of Sz 114. The only detected atomic/ionic line in the spectrum of Sz 114 is that from [Ne II] at 12.81 μm (see Table 2). The H_2 peak centroids are consistent with the stellar radial velocity, while the [Ne II] is clearly blueshifted; see Figure 3. A discussion of the H_2 and [Ne II] lines is provided in Appendix B. Here, we focus on the prominent water lines and the CO_2, C_2H_2, and HCN rovibrational bands.

4. Sz 114 in the Context of Other Disks

As described in Section 3, the MIRI-MRS spectrum of Sz 114 is dominated by molecular emission, especially from water vapor. As such, its spectrum is very different from that of late M-star disks observed with Spitzer/IRS and more similar to that of disks around earlier-type stars. To better illustrate the difference, we show in Figure 4 line flux ratios with respect to water emission at 17.22 μm, scaled at 160 pc. We focus on C_2H_2, HCN, and CO_2, as these rovibrational bands were previously detected in Spitzer/IRS, and their fluxes or upper limits are tabulated. The sample of late M-type stars is from Pascucci et al. (2013) and includes at most six sources with SpTy M7.25−M4.5 for which line flux ratios (including upper or lower limits) can be calculated. The sample of earlier-type stars (M3−G0) is from Banzatti et al. (2020) and includes at
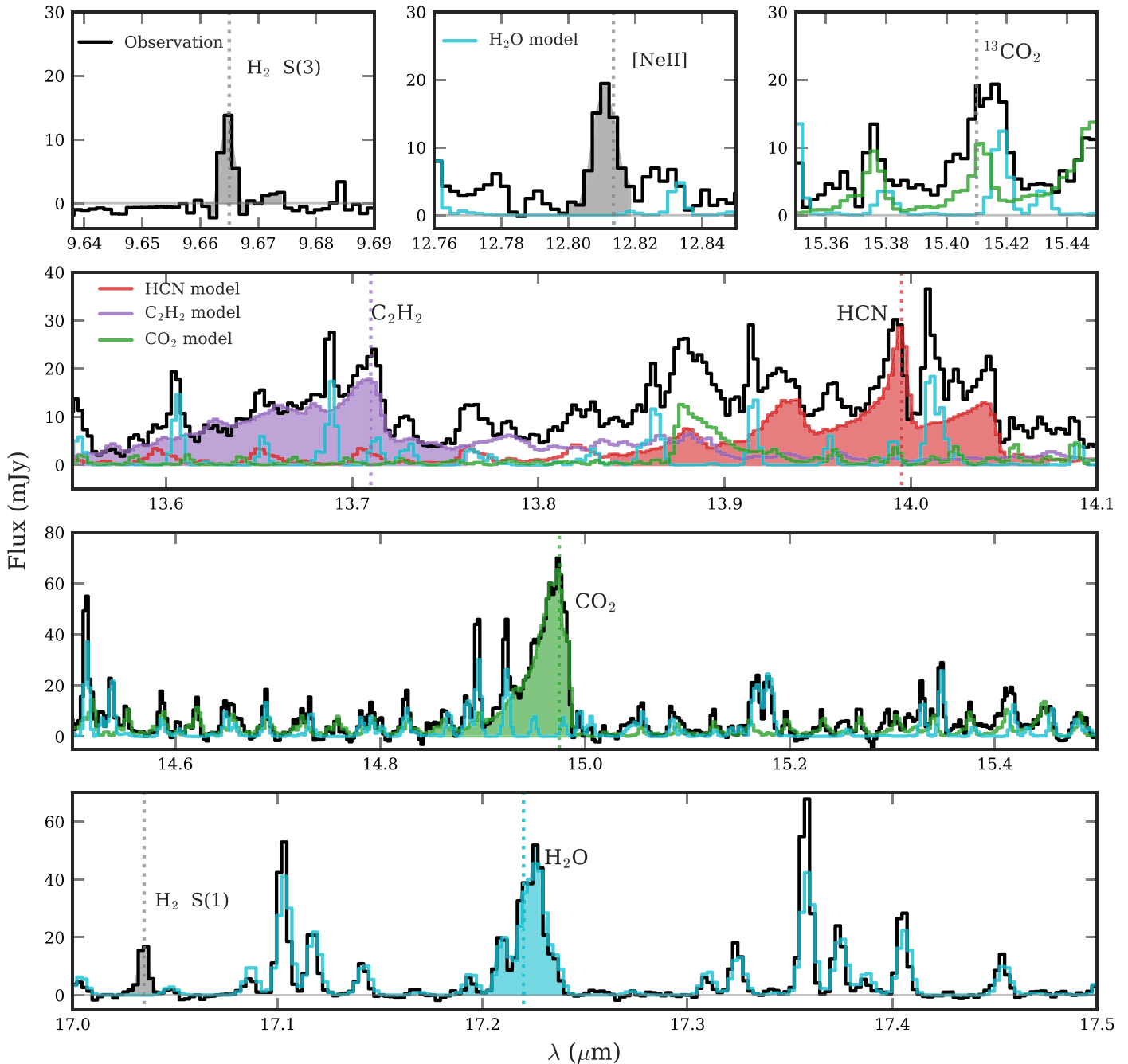
Figure 3. Expanded view of wavelength regions covering the ionic, atomic, and molecular lines reported in Table 2. Shaded regions indicate the wavelength ranges over which fluxes are measured. For C_2H_2 (purple), HCN (red), and CO_2 (green), these are the same ranges as those adopted in earlier Spitzer/IRS studies to facilitate comparison with literature sources. For H_2O (light blue), the wavelength range is restricted to the complex around 17.22 μm. The best-fit spectra obtained with CLIcK are also shown with solid lines.

most 49 sources.[20] For this latter sample, we note that the water line flux has been recalculated using the restricted wavelength range around the 17.22 μm transition.

Figure 4 demonstrates that Sz 114 has an unusually strong 17.22 μm water flux for its late SpTy compared to other mid-to-late M-star disks observed before, more similar to that of disks around early M- and K-type stars. The only other outlier in this sample is the disk of XX Cha, a slightly earlier SpTy source (M3.5) observed with Spitzer/IRS and more recently with JWST/MIRI but whose MIRI spectrum has not been published

yet. Additionally, Sz 114 shares similar HCN/H_2O and C_2H_2/H_2O flux ratios with XX Cha, both of which fall well within the range of values observed in disks around earlier-type stars. One difference is the slightly higher CO_2/H_2O flux ratio exhibited by Sz 114. In contrast to Sz 114, late M-star disks tend to have higher C_2H_2/H_2O flux ratios (Figure 4, lower panel) and higher C_2H_2/HCN ratios (see Figure 13 from Pascucci et al. 2009). These higher ratios have been attributed to a very high C/O ratio ($\geqslant 0.8$) in the inner disk of late M-type stars (Pascucci et al. 2013; Tabone et al. 2023), as the extra carbon that does not end up in CO can efficiently form hydrocarbons in the gas phase (e.g., Najita et al. 2011). Sz 114

---

[20] The source number is different among panels because of nondetections.

Table 1
Properties of Sz 114 Relevant to This Work

Property (Unit)	Value	References
Distance (pc)	156.8 ± 0.6	1, 3
Spectral type	M5	2
L_* ($L_\odot$)	0.196	2, 3
M_* ($M_\odot$)	0.16	2, 3
$\log(\dot{M})$ ($M_\odot$ yr^{-1})	-9.1	2, 3
$\log(L_{acc})$ ($L_\odot$)	-2.7	2, 3
$F_{0.89\ mm}$ (mJy)	96.41	4
Disk inclination (deg)	21.3 ± 1.3	5
R_{dust} (au)	$56^a \pm 1$	5

Note. 1. Gaia Collaboration et al. (2021); 2. Alcalá et al. (2017); 3. Manara et al. (2023); 4. Ansdell et al. (2016); 5. Huang et al. (2018).
[a] Scaled to the Gaia distance in this table.

Table 2
Summary of Line Fluxes

Species	λ-range (μm)	Flux (10^{-14} erg s^{-1} cm^{-2})	Comments
Atomic and Ionic			
[Ne II]	12.80–12.82	0.3	
Molecular			
CO (P35 1-0)	5.024–5.031	1.07	
H$_2$ (0,0) S(3)	9.66–9.675	0.12	
H$_2$ (0,0) S(1)	17.02–17.045	0.07	
C$_2$H$_2$	13.553–13.764	2.12	[a]
HCN	13.837–14.075	2.23	[a]
CO$_2$	14.847–15.014	3.61	[a]
^{13}CO$_2$	15.39–15.43	0.19	[b]
H$_2$O	17.19–17.25	0.87	

Notes. Sz 114 has a forest of water emission lines. We first fit the water spectrum and subtract the best-fit water model before computing the flux from other species or fitting the emission from other molecular lines.
[a] Emission from these species is blended; hence, we use our best-fit model flux here.
[b] This is a tentative detection after subtracting blended water and ^{12}CO$_2$ lines.

clearly shows that there is a larger diversity of mid-IR spectra down to late spectral types than previously inferred from the Spitzer/IRS surveys.

To place the Sz 114 system into context, we have also collected the accretion luminosity (L_{acc}) and millimeter flux (F_{mm}) for the earlier spectral type sample (Banzatti et al. 2020) and an expanded late M-star disk sample that now includes systems observed at the lowest Spitzer/IRS resolution ($R \sim 100$) from Pascucci et al. (2009); see Figure 5. This latter sample had, on average, a higher C$_2$H$_2$/HCN flux ratio than disks around earlier-type stars, but nothing could be said about the strength of the water emission due to the very low spectral resolution. The L_{acc} and F_{mm} from this expanded sample are from Manara et al. (2023), who homogenize measurements from various surveys (e.g., Andrews et al. 2013; Ansdell et al. 2016; Pascucci et al. 2016; Alcalá et al. 2017). The reason for focusing on these two parameters is that multiple Spitzer studies have shown that water emission is positively correlated with accretion luminosity (e.g., Salyk et al. 2011; Banzatti et al. 2020), while the water/HCN ratio is anticorrelated with the disk millimeter flux (Najita et al. 2013). Banzatti et al. (2020)

also found that the water/HCN ratio, as well as the water luminosity corrected for the L_{acc} trend, is anticorrelated with the dust disk radius as millimeter fluxes are correlated with dust disk sizes (e.g., Tripathi et al. 2017; Hendler et al. 2020).

The positive correlation between water and accretion luminosity is likely driven by the additional heating that accretion can provide for the excitation of the lines (e.g., Glassgold et al. 2009; Najita & Ádámkovics 2017). Indeed, the luminosity of several other infrared lines is also positively correlated with L_{acc} (e.g., Salyk et al. 2011 and Figure 8). The anticorrelation between the water and millimeter flux (and dust disk size) has been interpreted in the context of the pebbles' drift; low millimeter fluxes might result from the efficient inward drift of icy pebbles (roughly the millimeter-sized grains detected by ALMA), which increase the water vapor in the inner disk upon crossing the snowline (Banzatti et al. 2020). This scenario is supported by new MIRI spectra showing excess cold water emission in compact disks, which could originate from enhanced ice sublimation due to a larger flux of inward-drifting pebbles (Banzatti et al. 2023a).

As seen in Figure 5, Sz 114 has a relatively large accretion luminosity for its spectral type, further supporting the expectation that extra heating boosts infrared lines, including from H$_2$O. However, Sz 114 and J160532 do not follow the anticorrelation between water luminosity and F_{mm}. The infrared spectrum of the millimeter-brighter, larger, and structured disk of Sz 114 is significantly more water-rich than that of the millimeter-faint J160532. Note that the spectral type, as well as the stellar mass and accretion luminosity, of these two objects are strikingly similar (see Figure 5). One major difference, in addition to the millimeter flux (and potential size and substructures), is the likely age of the two objects; Sz 114 belongs to the $\sim$1–3 Myr old Lupus star-forming region (Galli et al. 2020) and has an isochronal age of $\sim$1 Myr (Alcalá et al. 2017), while J160532 belongs to the $\sim$5–10 Myr old Upper Sco association (e.g., Preibisch & Mamajek 2008; Luhman & Esplin 2020) and has a dynamical age of 2.5 ± 1.6 Myr (Miret-Roig et al. 2022). With the same spectral type but a stellar luminosity that is $\sim$5 times lower than that of Sz 114, J160532 is clearly older.

How might age play a role in explaining the different mid-IR spectra? Recently, Mah et al. (2023) carried out simulations using a coupled disk evolution and planet formation code that includes pebble drift and evaporation at ice lines in radially smooth disks (that is, a disk with no gaps or pressure bumps). They showed that, for such disks, the C/O ratio inside the snowline initially decreases below the stellar value due to the inward drift and evaporation of water ice–rich pebbles before it increases to superstellar values due to the inward diffusion of carbon-rich vapor, mostly from the evaporation of CH$_4$, from the accreting gas surface flow. Importantly, the transition from low to high C/O ratios (water-rich to water-poor) occurs faster around very low mass stars because of the closer-in ice lines (e.g., Mulders et al. 2015), shorter viscous timescales, and faster radial drift (e.g., Pinilla et al. 2013). Specifically, Mah et al. (2023) estimated that the inner disk of a 0.1 $M_\odot$ star dries out in $\sim$0.5 Myr if the α viscosity is 10^{-3} and $\sim$2 Myr for $\alpha = 10^{-4}$, while that of a 0.7 $M_\odot$ star dries out in $\sim$2 and $\sim$10 Myr, respectively (see their Figure 1). This scenario explains the general trend that the inner disks of late M stars are relatively more water-poor (C-rich) than similarly aged disks around earlier-type stars, as well as the difference in the
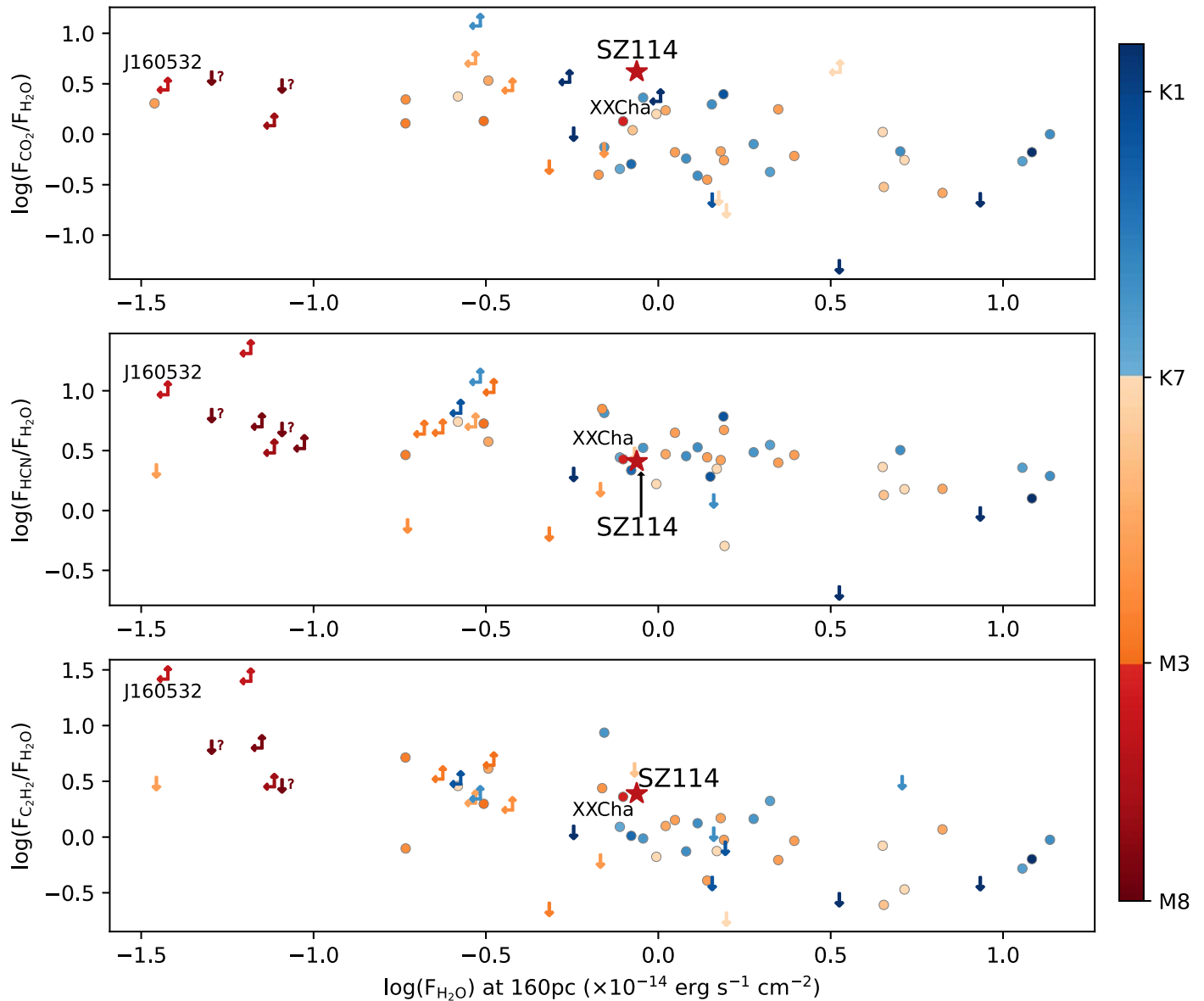
Figure 4. Molecular flux ratios vs. scaled water flux for mid-to-late M-star disks (Pascucci et al. 2013) and disks around earlier-type stars (Banzatti et al. 2020). In these comparisons, the water line at 17.22 μm is adopted. The two downward arrows with a question mark next to them are for the tentative Spitzer water detections in the mid-to-late M-star disks of J043814 and J044427. J160532 is a source similar to Sz 114 in spectral type, stellar mass, and accretion luminosity but is extremely carbon-rich. XX Cha is a slightly earlier-type (M3.5) star with a disk rich in water. Note how Sz 114 (star symbol) has more similar molecular flux ratios to earlier than later SpTy except for CO_2/H_2O, which is higher than the average earlier-type disk value.

spectra of Sz 114 and J160532. By the relatively later age of J160532, the icy pebble supply from the outer disk has likely been consumed (as suggested by the low millimeter flux), and the inner disk C/O ratio has been enhanced by the inner diffusion of carbon-rich vapor, which then triggers the formation of hydrocarbons. In contrast, at the early time of Sz 114, the inward drift of icy pebbles and the water vapor released when crossing the snowline, in combination with accretional heating, may boost the water emission. Interestingly, the two tentative detections of water in Spitzer/IRS spectra of similarly late M-star disks are also from young systems in the Taurus star-forming region (Pascucci et al. 2013).

While these ideas may account for the relative properties of Sz 114 and J160532, it is also interesting to consider why Sz 114 is so different from the majority of the mid-to-late

M-star disks of similar age observed with Spitzer/IRS. One possibility is that Sz 114 formed with unusual initial conditions, i.e., a large and massive disk at birth. Sz 114 has an exceptionally large millimeter flux and extended dust disk among mid-to-late M stars. Sz 114 may also be unusual among mid-to-late M-star disks in hosting substructures (gaps). The shallow gap detected by DSHARP at ~39 au, along with potential other substructures between ≈7 and 12 au, might maintain some icy pebbles further out, thus maintaining a large disk and, at the same time, prolonging water enrichment in the inner disk (see, e.g., Figure 4 in Kalyaan et al. 2023 for this effect in disks around solar-type stars). In contrast, most mid-to-late M-star disks are characterized by low millimeter fluxes (e.g., Pascucci et al. 2016 and Figure 5 for those targeted with Spitzer/IRS). These faint disks are low in the total number of icy pebbles; they might have started with an overall smaller and
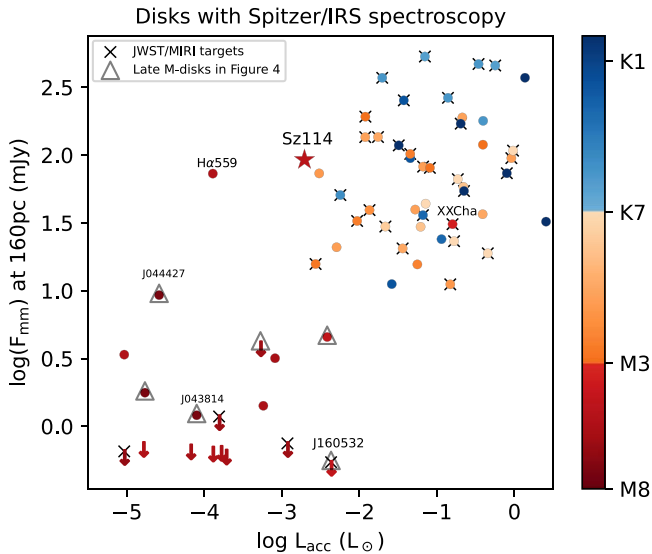
Figure 5. Flux at 0.89 mm scaled at 160 pc vs. accretion luminosity. Symbols are color-coded by SpTy. The sample of mid-to-late M-star disks includes those in Pascucci et al. (2009), which were only observed at the lowest Spitzer/IRS resolution. Down arrows indicate millimeter upper limits. Triangles are for the mid-to-late M-star disks present in Figure 4, while crosses indicate JWST/MIRI targets. Sz 114 is indicated with a star and shows a significantly higher millimeter flux than other mid-to-late M-star disks observed with Spitzer/IRS.

less massive disk than Sz 114 and have not developed any substructure to slow down the inner drift of icy pebbles. As a result, the typical inner disk of late M stars would follow the evolution described in Mah et al. (2023) and "dry out" fast, as discussed above. A sketch that places the temporal evolution of the C/O ratio in context for both Sz 114 and other late M-star disks is provided in Figure 6.

These ideas can be tested with MIRI-MRS spectroscopy of larger samples of disks surrounding mid-to-late M stars. JWST GTO and GO Cycle 1 and 2 programs will also cover the low millimeter flux disks around late M stars (see crosses in Figure 5) for which, similar to J160532, we expect water-poor and C-rich spectra even at young ages. It would be valuable to carry out MIRI-MRS observations of the late M-star disk in Taurus with tentative water detection and moderately high F_{mm} (J044427), as well as of ESO Hα 559, which has a millimeter flux comparable to Sz 114. If our interpretation of the data at hand is correct, we expect these spectra to be as water-rich as the spectrum of Sz 114. Fully testing the proposed scenario would require sensitive MIRI-MRS spectra of disks spanning a large range in spectral type, millimeter fluxes, accretion luminosities, and ages across several star-forming regions.

5. Summary and Outlook

We have acquired and analyzed the JWST/MIRI-MRS spectrum of Sz 114, an accreting M5 star in the ~1–3 Myr old Lupus star-forming region surrounded by a class II disk. This system has a high millimeter flux and was selected for DSHARP, which discovered a large dust disk with a size of ~58 au and a shallow gap at ~39 au. Additional unresolved substructures may also be present between ≈7 and 12 au (Jennings et al. 2022). This disk was not previously observed with Spitzer/IRS at $R \sim 700$; hence, there are no gas line detections previously reported. We model the MRS spectrum of Sz 114 with a slab of gas in LTE with the main goal of
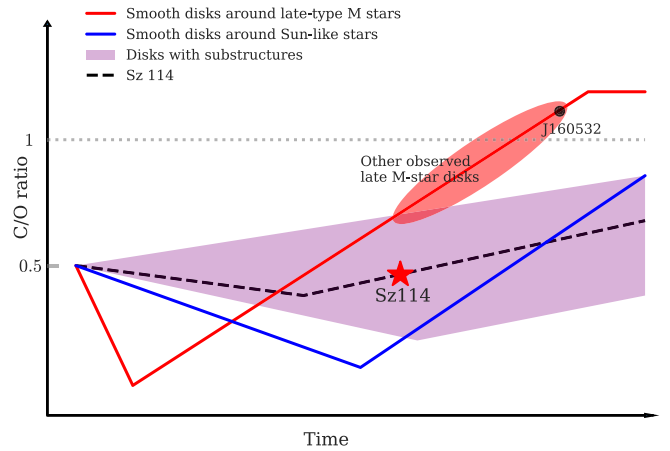
Figure 6. Sketch of the inner disk C/O ratio evolution with time. Substructures, depending on their locations and depths, can slow down the inward drift of icy pebbles. The time at which the C/O ratio starts to increase indicates the depletion time of the inner water-rich phase and depends on several factors, including stellar mass, initial disk size, mass, viscosity, and the presence and depth of substructures. Model predictions for disks with substructures around solar-type stars can be found in Kalyaan et al. (2023). Models for disks without substructures around stars of different masses are presented in Mah et al. (2023).

removing line blending and calculating fluxes for the detected gas lines. We also collect Spitzer/IRS fluxes from disks around stars of similar and earlier spectral type and discuss the spectrum of Sz 114 in the context of this larger sample. Our main results can be summarized as follows.

1. The MIRI-MRS spectrum of Sz 114 shows a forest of water emission lines, from the hot water bending rovibration band at ~6.6 μm through the cooler pure rotational lines at ~25 μm. In addition to water, we also detect CO, CO_2, HCN, and C_2H_2, with CO_2 having the strongest rovibrational band. Two H_2 lines and the [Ne II] at 12.81 μm are also robustly detected, while $^{13}CO_2$ is only marginally detected.

2. The water spectrum of Sz 114 between ~10 and 19 μm requires at least two LTE slabs of gas: hot close-in (~800 K) water emission and an additional cooler (~500 K) component whose emission comes from further out in the disk.

3. The 17.22 μm water flux of Sz 114 exceeds that of mid-to-late M-star disks, including that of the carbon-rich disk of J160532 observed with JWST, by an order of magnitude and falls within the range observed in disks around earlier-type stars by Spitzer. Similarly, the C_2H_2/H_2O and HCN/H_2O flux ratios of Sz 114 align with those of disks around earlier-type stars while exhibiting a slightly higher CO_2/H_2O ratio.

As for the earlier-type stars, most of the molecular emission from Sz 114 is expected to arise in the disk atmosphere inside the snowline. While accretion luminosity can boost molecular emission, it alone cannot account for the rich water spectrum observed in Sz 114; J160532, for example, exhibits a similar L_{acc} but a water-poor and C-rich spectrum. Several other factors might contribute to the exceptionally rich water spectrum of this late M-star disk. We have highlighted age because the water-rich inner disk phase is much shorter in smooth disks around lower-mass stars. This is because icy pebbles, which are O-rich, are depleted faster, and the inner disk C/O ratio is

enhanced earlier through the diffusion of C-rich vapor (Mah et al. 2023). Age could explain the difference between the MIRI spectra of Sz 114 and the relatively older J160532. In addition, we propose that unusual initial conditions, a large massive disk at birth, combined with the development of substructures, might be necessary to understand Sz 114 in the context of other mid-to-late M-star disks of similar age observed with Spitzer/IRS. The existence of the ~39 au shallow gap in the disk of Sz 114 might help to retain a large dust size, but it is not a strong enough barrier to pebbles drifting inward and could just help prolong the water-rich phase of the inner disk (Kalyaan et al. 2023). The other inferred substructures between ≈7 and 12 au might further delay the delivery of water vapor inside the midplane snowline, which is expected to be only ~0.1–0.5 au from the star. This delay would preserve a lower C/O ratio for a more extended period compared to other mid-to-late M-star disks, the majority of which are millimeter-faint and likely lack significant dust traps. The lower frequency of dust traps, in combination with a typically low disk mass at birth, could have important implications for the type of planets forming in disks around late M stars. For instance, in the context of planet formation via pebble accretion, Mulders et al. (2021) predict that the frequency of close-in super-Earths should decrease for $M_* \leqslant 0.5 M_\odot$, meaning that systems like TRAPPIST-1 would be rare.

Our findings demonstrate that the mid-infrared spectra of mid-to-late M-star disks exhibit greater diversity than previously inferred from the limited subset observed with Spitzer. This underscores the importance of expanding the sample size to comprehensively explore and better understand the potential range of variations.

Appendix A
Fitting Process and Error Bars

We apply a custom-written random walk process to fit the MIRI spectrum of Sz 114. The likelihood function is defined as follows (e.g., Hogg et al. 2010):

$$\ln(\mathcal{L}) = -\frac{1}{2}\sum_\lambda \left[\left(\frac{F_M(\lambda, \theta) - F_D(\lambda)}{s_D} \right)^2 + \ln(2\pi s_D^2) \right]. \quad (A1)$$

The $F_M(\lambda, \theta)$ is the flux of our model at λ with the parameter set $\theta(N, R_{em}, T)$, and $F_D(\lambda)$ is the continuum-subtracted JWST-MIRI data. $s_D^2 = \sigma_D^2 + f^2 (F_M(\lambda, \theta))^2$ indicates the variance of our data (Hogg et al. 2010), where σ_D is the uncertainty of the data and $f \times F_M(\lambda, \theta)$ is a factor accounting for a possible underestimation of the uncertainty. We simplify this process by ignoring this possible underestimation; i.e., we assume $f = 0$, and the likelihood is therefore simplified to $\ln(\mathcal{L}) = K - \frac{1}{2}\chi^2$, where $K = -\frac{1}{2}\sum_\lambda \ln(2\pi\sigma_D^2)$ is a constant and $\chi^2 = \sum_\lambda \left(\frac{F_M(\lambda, \theta) - F_D(\lambda)}{\sigma_D} \right)^2$. We also apply a flat prior inside the boundaries mentioned in Section 3 throughout our fitting.

Our random walk process works as follows. For each initial parameter set $\theta(N, R_{em}, T)$, we run a model with CLIcK and compare our model with the data to get a likelihood $\mathcal{L}(\theta)$. Then we "walk" the parameter set θ to eight different directions as $\theta_i(N \times \Delta N_i, R_{em} + \Delta R_{em,i}, T + \Delta T_i)$ and calculate the likelihood for each of them, $\mathcal{L}(\theta_i)$. The model with the largest likelihood among the eight models is chosen to be an "accepted model" and become the next initial parameter set. We repeat the process until the likelihood function settles to a certain value. The best-fit model is the model with the highest likelihood. This approach is similar to previous grid fittings that minimize χ^2 (e.g., Grant et al. 2023; Tabone et al. 2023). The error bars are determined through typical Markov Chain Monte Carlo methods, where 1σ uncertainties are chosen as the 16th and 84th percentile values from the distribution of parameter space spanned by our walkers (see Figure 7). Due to the overlapping emission, C_2H_2 and HCN are fitted together. The column density (N) and temperature (T) of the two molecules are highly degenerate with each other; thus, the error bars of the fitted parameters are very large and not shown here (e.g., Table 3). We note that our major goal is to separate the contribution from different molecules to calculate line fluxes

Table 3
Summary of Model Fitting

Species		λ-range (μm)	T (K)	$\log_{10}(N)$ (cm^{-2})	R_{em} (au)
H_2O	Hot	10–12	750^{+150}_{-130}	18.8 ± 0.4	0.17
	Cool	16.3–19	450^{+90}_{-60}	$18.2^{+0.8}_{-0.3}$	0.5
CO_2		14.6–15.4	500^{+200}_{-150}	$17.6^{+1.2}_{-1.1}$	0.18
C_2H_2		13.5–14.3	1400	15.5	0.42
HCN		13.5–14.3	870	15.9	0.39

Note. We identify two sets of well-fit parameters for C_2H_2 and HCN given the intrinsic degeneracies between column density, temperature, and emitting area in LTE slab models of warm gas in protoplanetary disks (e.g., Salyk et al. 2011; Najita et al. 2018). The values reported here correspond to the maximum likelihood in our fitting routine, and the other parameter set is $T \sim 400$ K and $\log_{10}(N) \sim 19$ cm^{-2} for both C_2H_2 and HCN.
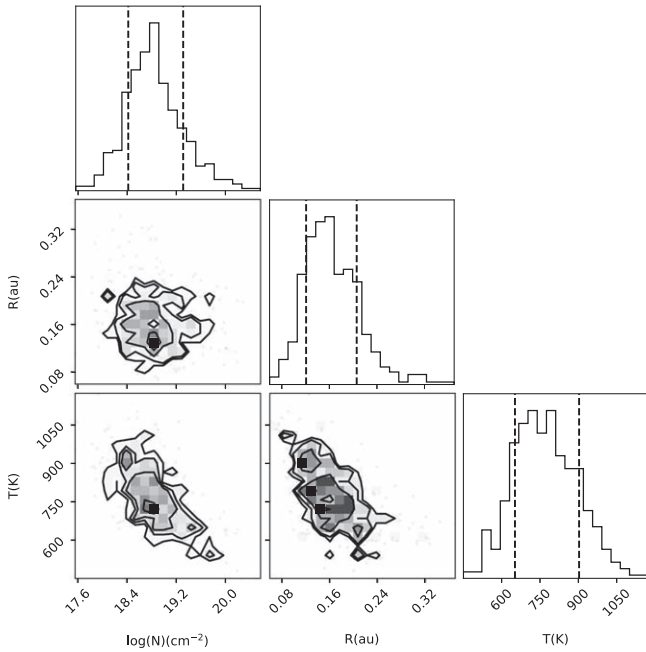
Figure 7. Corner plot of our hot water models as an example of our fitting. The vertical dashed lines indicate the 1σ of each parameter as the middle 68% of the accepted models. We can see the degeneracy between the three parameters from the shape of the distribution.

and use the strategies mentioned above to speed up our modeling. See Figures 2 and 3 for the comparison between our fitted models and the data.

Appendix B
[Ne II] and H₂ Emission

As mentioned in Section 3, we have detected two molecular hydrogen transitions, both with peak centroids consistent with the stellar radial velocity: the S(3) at $\sim9.67\ \mu$m and the S(1) at $\sim17.035\ \mu$m. The critical densities of these two lines are low (Mandy & Martin 1993) compared with the typical density of protoplanetary disks in the H₂ emitting region (e.g., Woitke et al. 2009). Therefore, the population levels are likely to be in LTE. With the further assumption that the emission is optically thin, we use Equation (1) in Lahuis et al. (2007) and derive a temperature of ~425 K from their line ratio, which is consistent with temperatures near the disk surface (e.g., Kamp & Dullemond 2004; Woitke et al. 2018).

Sz 114 also has a fairly strong [Ne II] 12.81 μm detection for its spectral type. In Figure 8, we compare its line luminosity to that of other late M-star disks (Pascucci et al. 2013) and disks around earlier-type stars (Banzatti et al. 2020) as a function of accretion luminosity ($L_{\rm acc}$). [Ne II] fluxes for the disks around earlier-type stars are collected from Güdel et al. (2010) and Rigliaco et al. (2015), and luminosities are computed using the most updated Gaia DR3 distances (Gaia Collaboration et al. 2021). Sz 114 is not only bright in the [Ne II] line for its spectral type but also brighter than the average for sources with the same $L_{\rm acc}$. This hints at extra [Ne II] emission from a jet (e.g., Güdel et al. 2010), which is supported by the 70 km s^{-1} blueshift in the peak centroid with respect to stellar radial velocity. A high-velocity blueshifted component is also detected in the [O I] 6300 Å profile obtained with the X-Shooter/VLT (Nisini et al. 2018). A visual inspection of the MIRI-MRS data cube around the [Ne II] line does not show
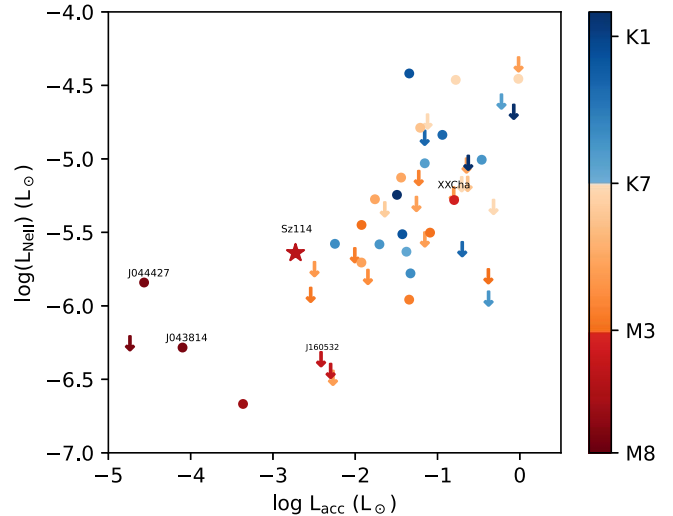
Figure 8. [Ne II] vs. accretion luminosities for the sample of late M-type (Pascucci et al. 2013) and disks around earlier-type stars (Banzatti et al. 2020). For the latter sample, [Ne II] fluxes are collected from Güdel et al. (2010) and Rigliaco et al. (2015).

any extension, possibly due to the almost face-on (21°; Huang et al. 2018) disk inclination. More detailed analysis of the MIRI-MRS data cubes and/or higher-S/N exposures might reveal a spatially resolved [Ne II] jet and enable measurement of the proportion of jet versus disk emission.

ORCID iDs

Chengyan Xie ⬤ https://orcid.org/0000-0001-8184-5547
Ilaria Pascucci ⬤ https://orcid.org/0000-0001-7962-1683
Feng Long ⬤ https://orcid.org/0000-0002-7607-719X
Klaus M. Pontoppidan ⬤ https://orcid.org/0000-0001-7552-1562
Andrea Banzatti ⬤ https://orcid.org/0000-0003-4335-0900
Anusha Kalyaan ⬤ https://orcid.org/0000-0002-5067-1641
Colette Salyk ⬤ https://orcid.org/0000-0003-3682-6632
Yao Liu ⬤ https://orcid.org/0000-0002-7616-666X
Joan R. Najita ⬤ https://orcid.org/0000-0002-5758-150X
Paola Pinilla ⬤ https://orcid.org/0000-0001-8764-1780
Nicole Arulanantham ⬤ https://orcid.org/0000-0003-2631-5265
Gregory J. Herczeg ⬤ https://orcid.org/0000-0002-7154-6065
John Carr ⬤ https://orcid.org/0000-0002-6695-3977
Edwin A. Bergin ⬤ https://orcid.org/0000-0003-4179-6394
Nicholas P. Ballering ⬤ https://orcid.org/0000-0002-4276-3730
Sebastiaan Krijt ⬤ https://orcid.org/0000-0002-3291-6887
Geoffrey A. Blake ⬤ https://orcid.org/0000-0003-0787-1610
Ke Zhang ⬤ https://orcid.org/0000-0002-0661-7517
Karin I. Öberg ⬤ https://orcid.org/0000-0001-8798-1347
Joel D. Green ⬤ https://orcid.org/0000-0003-1665-5709

References

Alcalá, J. M., Manara, C. F., Natta, A., et al. 2017, A&A, 600, A20
Andrews, S. M., Huang, J., Pérez, L. M., et al. 2018, ApJL, 869, L41
Andrews, S. M., Rosenfeld, K. A., Kraus, A. L., & Wilner, D. J. 2013, ApJ, 771, 129
Ansdell, M., Williams, J. P., Trapman, L., et al. 2018, ApJ, 859, 21
Ansdell, M., Williams, J. P., van der Marel, N., et al. 2016, ApJ, 828, 46
Apai, D., Pascucci, I., Bouwman, J., et al. 2005, Sci, 310, 834

Astropy Collaboration, Price-Whelan, A. M., Lim, P. L., et al. 2022, ApJ, 935, 167
Astropy Collaboration, Price-Whelan, A. M., Sipőcz, B. M., et al. 2018, AJ, 156, 123
Astropy Collaboration, Robitaille, T. P., Tollerud, E. J., et al. 2013, A&A, 558, A33
Bae, J., Isella, A., Zhu, Z., et al. 2023, in ASP Conf. Ser. 534, Protostars and Planets VII, ed. Inutsuka Shu-ichiro et al. (San Francisco, CA: ASP), 423
Banzatti, A., Pascucci, I., Bosman, A. D., et al. 2020, ApJ, 903, 124
Banzatti, A., Pontoppidan, K. M., Carr, J., et al. 2023a, ApJL, 957, L22
Banzatti, A., Pontoppidan, K. M., Pére Chávez, J., et al. 2023b, AJ, 165, 72
Bean, J. L., Raymond, S. N., & Owen, J. E. 2021, JGRE, 126, e06639
Bushouse, H., Eisenhamer, J., Dencheva, N., et al. 2022, JWST Calibration Pipeline, v1.6.2, Zenodo, doi:10.5281/zenodo.7041998
Carr, J. S., & Najita, J. R. 2011, ApJ, 733, 102
Galli, P. A. B., Bertout, C., Teixeira, R., & Ducourant, C. 2013, A&A, 558, A77
Gaia Collaboration, Brown, A. G. A., Vallenari, A., et al. 2021, A&A, 649, A1
Galli, P. A. B., Bouy, H., Olivares, J., et al. 2020, A&A, 643, A148
Glassgold, A. E., Meijerink, R., & Najita, J. R. 2009, ApJ, 701, 142
Gordon, I. E., Rothman, L. S., Hargreaves, R. J., et al. 2022, JQSRT, 277, 107949
Grant, S. L., van Dishoeck, E. F., Tabone, B., et al. 2023, ApJL, 947, L6
Güdel, M., Lahuis, F., Briggs, K. R., et al. 2010, A&A, 519, A113
Hendler, N., Pascucci, I., Pinilla, P., et al. 2020, ApJ, 895, 126
Hogg, D. W., Bovy, J., & Lang, D. 2010, arXiv:1008.4686
Huang, J., Andrews, S. M., Dullemond, C. P., et al. 2018, ApJL, 869, L42
Hughes, J., Hartigan, P., Krautter, J., & Kelemen, J. 1994, AJ, 108, 1071
Izidoro, A., Schlichting, H. E., Isella, A., et al. 2022, ApJL, 939, L19
Jennings, J., Booth, R. A., Tazzari, M., Clarke, C. J., & Rosotti, G. P. 2022, MNRAS, 509, 2780
Kalyaan, A., Pinilla, P., Krijt, S., et al. 2023, ApJ, 954, 66
Kamp, I., & Dullemond, C. P. 2004, ApJ, 615, 991
Lahuis, F., van Dishoeck, E. F., Blake, G. A., et al. 2007, ApJ, 665, 492
Liu, Y., Pascucci, I., & Henning, T. 2019, A&A, 623, A106
Luhman, K. L., & Esplin, T. L. 2020, AJ, 160, 44
Mah, J., Bitsch, B., Pascucci, I., & Henning, T. 2023, A&A, 677, L7
Manara, C. F., Ansdell, M., Rosotti, G. P., et al. 2023, in ASP Conf. Ser. 534, Protostars and Planets VII, ed. Inutsuka Shu-ichiro et al. (San Francisco, CA: ASP), 539
Mandell, A. M., Bast, J., van Dishoeck, E. F., et al. 2012, ApJ, 747, 92
Mandy, M. E., & Martin, P. G. 1993, ApJS, 86, 199

Miret-Roig, N., Galli, P. A. B., Olivares, J., et al. 2022, A&A, 667, A163
Mortier, A., Oliveira, I., & van Dishoeck, E. F. 2011, MNRAS, 418, 1194
Mulders, G. D., Ciesla, F. J., Min, M., & Pascucci, I. 2015, ApJ, 807, 9
Mulders, G. D., Drążkowska, J., van der Marel, N., Ciesla, F. J., & Pascucci, I. 2021, ApJL, 920, L1
Najita, J. R., & Ádámkovics, M. 2017, ApJ, 847, 6
Najita, J. R., Ádámkovics, M., & Glassgold, A. E. 2011, ApJ, 743, 147
Najita, J. R., Carr, J. S., Pontoppidan, K. M., et al. 2013, ApJ, 766, 134
Najita, J. R., Carr, J. S., Salyk, C., et al. 2018, ApJ, 862, 122
Natta, A., Testi, L., Calvet, N., et al. 2007, in Protostars and Planets V, ed. B. Reipurth, D. Jewitt, & K. Keil (Tucson, AZ: Univ. of Arizona Press), 767
Nisini, B., Antoniucci, S., Alcalá, J. M., et al. 2018, A&A, 609, A87
Öberg, K. I., & Bergin, E. A. 2021, PhR, 893, 1
Pascucci, I., Apai, D., Luhman, K., et al. 2009, ApJ, 696, 143
Pascucci, I., Herczeg, G., Carr, J. S., & Bruderer, S. 2013, ApJ, 779, 178
Pascucci, I., Testi, L., Herczeg, G. J., et al. 2016, ApJ, 831, 125
Pegues, J., Öberg, K. I., Bergner, J. B., et al. 2021, ApJ, 911, 150
Pinilla, P., Birnstiel, T., Benisty, M., et al. 2013, A&A, 554, A95
Pontoppidan, K. M., Salyk, C., Banzatti, A., et al. 2023, arXiv:2311.17020
Pontoppidan, K. M., Salyk, C., Bergin, E. A., et al. 2014, in Protostars and Planets VI, ed. H. Beuther et al. (Tucson, AZ: Univ. of Arizona Press), 363
Pontoppidan, K. M., Salyk, C., Blake, G. A., & Käufl, H. U. 2010, ApJL, 722, L173
Preibisch, T., & Mamajek, E. 2008, in Handbook of Star Forming Regions, Volume II, ed. B. Reipurth, Vol. 5 (San Francisco, CA: ASP), 235
Rieke, G. H., Wright, G. S., Böker, T., et al. 2015, PASP, 127, 584
Rigliaco, E., Pascucci, I., Duchene, G., et al. 2015, ApJ, 801, 31
Salyk, C., Lacy, J., Richter, M., et al. 2019, ApJ, 874, 24
Salyk, C., Pontoppidan, K. M., Blake, G. A., Najita, J. R., & Carr, J. S. 2011, ApJ, 731, 130
Tabone, B., Bettoni, G., van Dishoeck, E. F., et al. 2023, NatAs, 7, 805
Thi, W. F., Kamp, I., Woitke, P., et al. 2013, A&A, 551, A49
Tripathi, A., Andrews, S. M., Birnstiel, T., & Wilner, D. J. 2017, ApJ, 845, 44
van der Plas, G., van den Ancker, M. E., Waters, L. B. F. M., & Dominik, C. 2015, A&A, 574, A75
Virtanen, P., Gommers, R., Burovski, E., et al. 2020a, scipy/scipy: SciPy, v1.5.3, Zenodo, doi:10.5281/zenodo.4100507
Virtanen, P., Gommers, R., Oliphant, T. E., et al. 2020b, NatMe, 17, 261
Walsh, C., Nomura, H., & van Dishoeck, E. 2015, A&A, 582, A88
Wells, M., Pel, J. W., Glasse, A., et al. 2015, PASP, 127, 646
Woitke, P., Kamp, I., & Thi, W. F. 2009, A&A, 501, 383
Woitke, P., Min, M., Thi, W. F., et al. 2018, A&A, 618, A57